Characteristics of tidal-bore deposits and facies associations in the QiantangEstuary, China

Article *in* Marine Geology · November 2013

DOI: 10.1016/j.margeo.2013.11.012

Marine Geology 348 (2014) 1–14

Contents lists available at ScienceDirect

Marine Geology

journal homepage: www.elsevier.com/locate/margeo

Characteristics of tidal-bore deposits and facies associations in the Qiantang Estuary, China

Daidu Fan *, Junbiao Tu, Shuai Shang, Guofu Cai

State Key Laboratory of Marine Geology, Tongji University, Shanghai 200092, China

ARTICLE INFO

Article history:
Received 17 June 2013
Received in revised form 15 November 2013
Accepted 19 November 2013
Available online 26 November 2013

Communicated by J.T. Wells

Keywords:
tidal bore
tidal rhythmite
sedimentary features
size composition
facies associations
Qiantang Estuary

ABSTRACT

The characteristics of tidal-bore deposition in the Qiantang Estuary are studied on the basis of core strata and grain-size data, and lateral and longitudinal associations with other sedimentary facies are synthesized. A typical depositional package by tidal bores and associated flows is generally initiated with (1) an undular/planar erosion base, overlain by (2) a massive sandy bed, and (3) a sandy bed with parallel laminations or some thinly heterolithic beds. The depositional units, especially the parallel laminations, are prone to deformation into convolute bedding, flames, and boiled sand patches with water-escape structures. In the middle estuary, tidal-bore deposits (TBDs) at the main channel and the lower tidal flat transit laterally into alternative beds of TBDs andz heterolithic beds at the middle tidal flat, and then toward incomplete tidal rhythmites on the higher tidal flat. TBDs are generally coarser and less sorted than tidal sandy deposits (TSDs), and tidal muddy deposits (TMDs) have finer grains, less sorting and lower positive skewness than either TSDs or TBDs. Therefore, bivariate plotting of size parameters is a useful tool to differentiate between these three genetic sedimentary bed types. Along the axis, three facies divisions are obvious and consist of: (1) linear depositional ridges and erosion troughs at the outer estuary, (2) TBDs at the middle estuary, and (3) coarse fluvial deposits at the upper estuary. The tripartite facies model of the Qiantang Estuary is similar to other well-known tide-dominated estuarine facies models, but it is the first to stress tidal-bore deposition in the sedimentary facies using detailed discriminative textural and structural characteristics. The approaches offer the potential to better understand tidal-bore processes and their important role in sediment dispersion and facies formation within modern and ancient macrotidal to hypertidal estuaries.

1. Introduction

A tidal bore is a moving hydraulic jump, triggered by a rushing flood tide into a funnel-shaped river mouth. The incoming tidal wave is amplified landward by a narrowing cross-bay section to achieve macrotidal (spring tidal range (STR) 4–6 m) or hypertidal (STR >6 m, Archer, 2013) conditions at the bay head, with increasing asymmetry in speeds and durations of tidal currents (Wells, 1995). As it propagates into a single tidal–fluvial channel with uplifted bed, the wave front can be further distorted to form a steep rising water wall known as a tidal bore. Borehead height varies from a few decimeters to a few meters in different rivers (Chanson, 2012). Tidal bores are classified into undular and breaking types based on their shapes. The undular bore potentially occurs under a tidal-bore Froude Number (Fr_1, referencing Chanson, 2012 for the definition and calculation formula) larger than 1.0, while a breaking bore is formed when Fr_1 exceeds 1.7–1.8 (Lin, 2008; Chanson, 2012).

Tidal bores occur at over 80 river mouths in the world (Bartsch-Winkler and Lynch, 1988). The most spectacular bores are those in the Qiantang Estuary (China), the Amazon Delta (Brazil), and the Turnagain Arm of Cook Inlet (Alaska), where rolling and breaking bores are at least 1 m high. The massive hydraulic power of tidal bores can exert a great impact on the estuarine ecosystem, sediment and pollutant dispersion, and waterway and infrastructure stability. Coastal engineers have paid much attention to the potential hazards of tidal bores over the last decade, studying bore hydro- and sediment-dynamic processes through field observations (Wolanski et al., 2001; Simpson et al., 2004; Chanson et al., 2011), flume experiments (Donnelly and Chanson, 2005; Koch and Chanson, 2008), and numerical modeling (Madsen et al., 2005; Pan et al., 2007; Lubin et al., 2010). Consequently, tidal bores and the subsequent rapid flows are known to reach an upper-flow regime, and turbulent flows are intensely mixed with the Reynolds Number (R_e) of 10^4 and higher (Chanson, 2009).

Some macrotidal-hypertidal estuaries fostering tidal bores have been extensively studied to formulate facies models of tide-dominated estuaries. They include the Cobequid Bay–Salmon River Estuary (Dalrymple et al., 1990, 1992), the Bristol Channel–Severn River Estuary (Harris, 1988; Allen, 1990), the Gironde Estuary (Allen, 1991; Allen and Posamentier, 1993), and the Mont-Saint-Michel Bay (Tessier, 1993,

* Corresponding author at: State Key Laboratory of Marine Geology, Tongji University, 1239 Siping Road, Shanghai 200092, China. Tel.: +86 21 65989073; fax: +86 21 65982208.
E-mail address: ddfan@tongji.edu.cn (D. Fan).

0025-3227/$ – see front matter © 2013 Published by Elsevier B.V.
http://dx.doi.org/10.1016/j.margeo.2013.11.012

2012). However, the known models for estuarine sedimentary facies and sequence stratigraphy do not provide typical imprints for tidal bores, possibly because the small bores in these estuaries are too weak to produce or preserve criteria that can be used to distinguish the tidal bores from other hydraulic processes. Pioneer work in the Mont-Saint-Michel Bay pointed out that soft-sediment deformation structures (like conical folds and round closed piles) in intertidal facies near the main channel result from liquefaction triggered by tidal-bore passages (Tessier and Terwindt, 1994). This innovative interpretation was recently extended to elucidate the formation of flow rolls, dish structures, flames and small dewatering pipes in the intertidal-flat deposits at the Turagain Arm, features which had been formerly ascribed to seismic events because of their earthquake-prone setting (Greb and Archer, 2007). Except for these multi-genesis soft-sediment deformation structures, the present knowledge of modern tidal-bore deposition is almost vacant, bewildering efforts to interpret fossil analogs. This was the situation when the authors pondered over the bore-genesis interpretation of a typical sedimentary package with an undular erosion surface overlain by homogeneous sands and bi-directional cross-bedded units in the Late Jurassic Lourinhã Formation (the Lusitanian Basin in Portugal, Martinius and Gowland, 2011).

In this paper 16 short cores collected primarily from the bore-affected tidal-fluvial channel section of the Qiantang Estuary were therefore studied in detail, aiming to (1) summarize diagnostic criteria of tidal-bore deposition in terms of textural and structural compositions, and (2) formulate a facies model of tide-dominated estuaries with tidal bores by synthesizing the association of tidal-bore deposits with other sedimentary facies along lateral and longitudinal coordinates.

2. Regional setting

The Qiantang River debouches into Hangzhou Bay, which has a gigantic funnel shape with a width of ~100 km at the bay mouth, and <20 km at the bay head (Fig. 1). A sharp decrease in bay width greatly deforms advancing tidal waves, by increasing the mean tidal range from <2 m at the mouth to ~5.5 m near Ganpu, where the mean and maximum spring tidal ranges reach 6.44 m and 9.00 m, respectively (Han et al., 2003; Lin, 2008; Fan, 2012). From there, tidal ranges decrease quickly upstream because of increasing friction by the elevated and narrowing river channel. The mean tidal range is 0.5 m at WY (Wen-Yan), about 115 km upstream of Ganpu (Fig. 1). The tidal limit is at LCB (Lu-Ci-Bu, station 11 in Fig. 2), where the water level can be

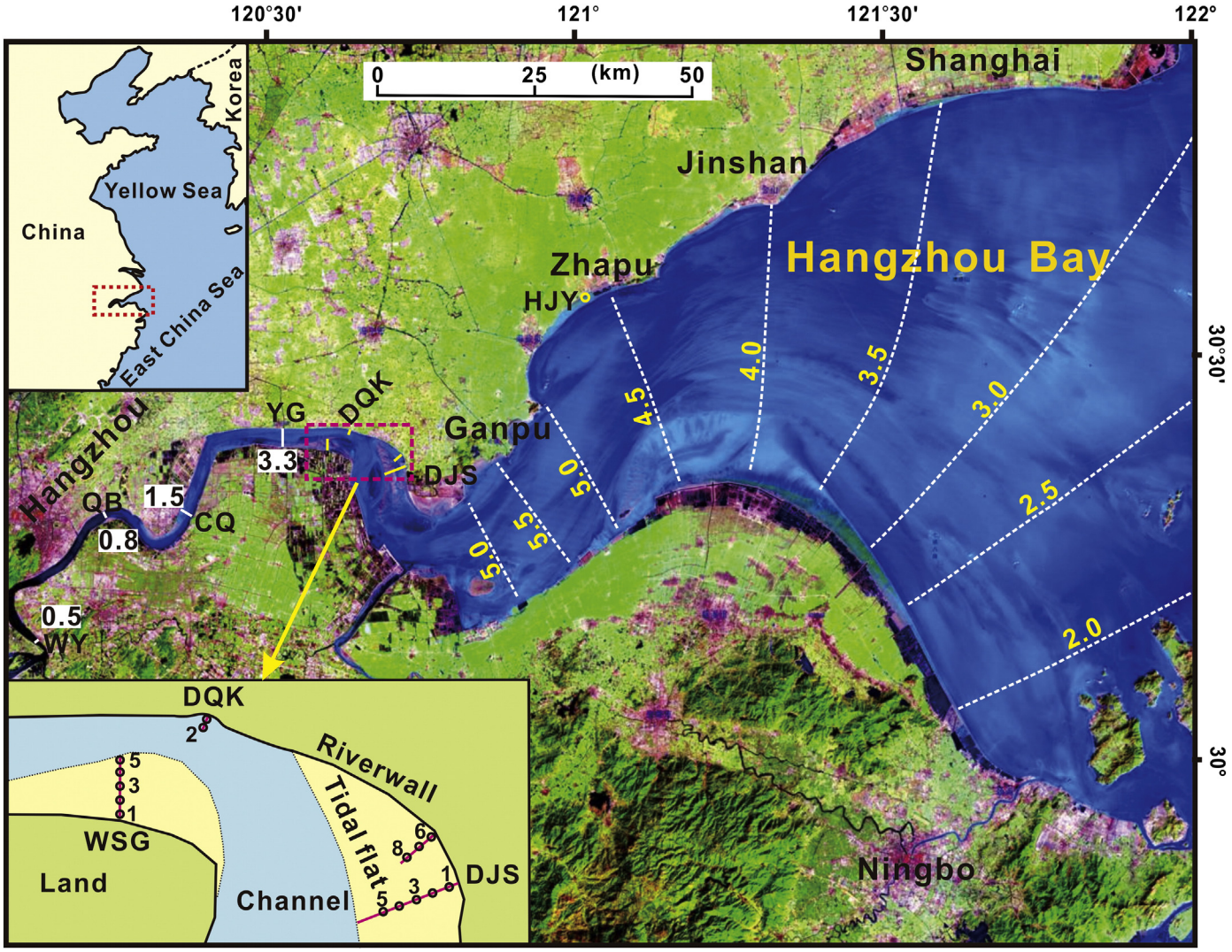

Fig. 1. Satellite photo of the Hangzhou Bay–Qiantang Estuary with co-range lines and sampling locations. Co-range lines and mean tidal ranges are shown as white broken lines or real lines with numbers. Fifteen short sediment cores were taken from three intertidal flats (DJS, DQK and WSG) neighboring the main channel subject to tidal bores, and another short core was collected from the upper intertidal flat near Zhapu, outside the bore-affected section.

raised by the backwater of spring tides, approximately 80 (280) km upstream of WY (the bay mouth). Long-term average salinity is 0.4‰ at ZK (Zha-Kou, station7 in Fig. 2), ~190 km upstream of the bay mouth. The reach between ZK and LCB is therefore a tidal-influenced freshwater river, referred to as the upper estuary in a tripartite division model (Chen et al., 1990; Zhang and Li, 1996; Lin et al., 2005).

Asymmetry in both speeds and durations of tidal currents increases progressively upstream within the estuary. The ratio of flooding and ebbing durations decreases slightly from one unit at the bay mouth to 0.84 at Ganpu, and then continues with a sharp drop to 0.34 at YG (Han et al., 2003). The ratio returns to a slow decreasing trend upstream of YG but ends with a slight increasing trend near the tidal limit (Fig. 2). The shorter flooding duration marks the flood domination of the bay and lower tidal river. The maximum depth-average speed of flooding (ebbing) currents reaches 3.80 (3.33) m/s at DJS, and 3.86 (2.34) m/s at YG according to field measurements during an intermediate tide, decreasing upstream and downstream from there (Han et al., 2003). Therefore, the axial peak flooding speed occurs 30–50 km upstream of the station having the maximum tidal range, and is related to the occurrence of raging bores in the middle estuary.

Tidal bores are usually bred at the middle ground between Ganpu and DJS because of the sharp decrease in both width and depth of the estuary where the rapid flow flushes from the open bay into a single sinuous channel. Water depth during low tides changes from >5 m at the front foot of the gigantic sand bar to <1 m at its top in the middle estuary (Chen et al., 1990; Han et al., 2003; Yu et al., 2012). The rapidly advancing tidal wave is further deformed and its front finally develops into undular surges. They grow upstream into breaking bores with a peak somewhere between DQK (Da-Que-Kou) and YG, and then decay upstream and finally disappear a little upstream of WY (Fig. 2). Therefore, the reach having tidal bores is roughly 100 km long. Bore head and height are clearly shown in tidal-level curves with a steep rise at the initiate flooding phase (Fig. 2). The maximum bore-head height is usually 2–3 m between DQK and YG, and this can potentially grow to 4 m or higher during special weather conditions, or through the action of interfering waves when the bore runs against the bank or river wall (Dai and Zhou, 1987; Pan and Huang, 2010; Fan et al., 2012). The Qiantang Estuary is one of only a few river mouths to breed tidal bores during neap tides because of high tidal speeds and typical channel morphology. Undular bores occur during neap tides and develop into breaking bores toward spring tides (Fig. 2).

The river reach breeding tidal bores in the middle estuarine section is highly sinuous, and markedly different from the straight upper and outer estuarine sections (Figs. 1, 2). The channel in the middle estuary was originally quite wide (20–30 km) and straight, with braided sand bars and extensive tidal flats that have been largely claimed in the last 300 years (Chen et al., 1990; Han et al., 2003). The man-made channel is now narrow and highly sinuous with well-developed point-bars along the meandering loops, usually within the lower-to-middle intertidal zones. The upper intertidal flat and marshland has been completely or partly obliterated by reclamation, and the remnants are typically very narrow with a steep front toward the middle intertidal flat (Fan et al., 2012). The thalweg sediment at the middle estuary is mainly composed of fine sands and coarse silts, in comparison with gravels and sands at the upper estuary. The depositional plain bed of the lower estuary consists primarily of silts with a few sands and clays, demarked by a few erosion troughs and accretion ridges which are composed of coarse sands with a few gravels and medium-fine sands with silts, respectively. The outer bay basin is covered predominantly by muds, sourced from the Yangtze (Changjiang) River plume (Chen et al., 1990; Zhang and Li, 1996; Han et al., 2003; Fan et al., 2012).

3. Materials and methods

3.1. Field and laboratory work

Several fieldtrips were carried out during the past few years in the middle estuary, including hydraulic surveys and short-core collections. Here we present the results of structural and textural composition analyses of 16 short cores. The short cores were collected from the intertidal zone during low tides by hand. PVC tubes (50–70 cm long) were hammered into the intertidal deposits, and then excavated with shovels. Sediment cores were firmly sealed in the tubes and taken back to the laboratory for analysis. Eight short cores (JS1–JS8) were taken from DJS tidal flats, the largest bank during the fieldtrip in May 2010 with a

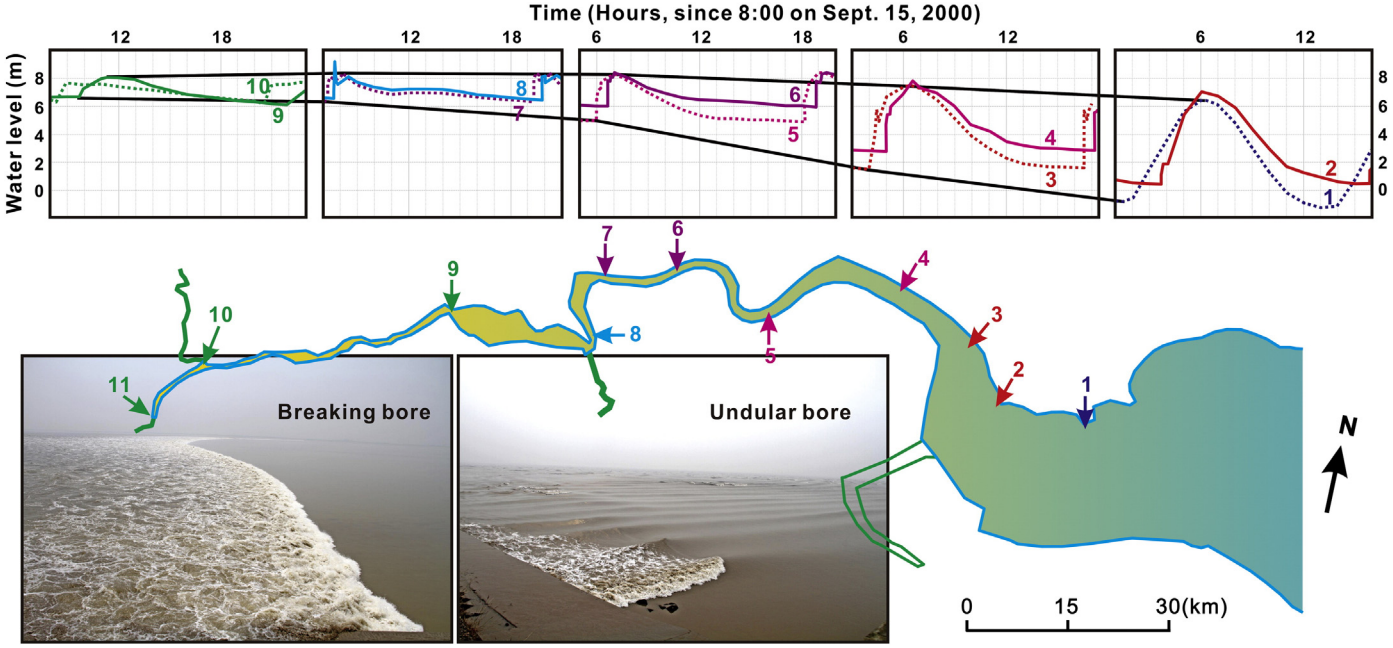

Fig. 2. Tidal asymmetry increases as it propagates upstream in the Qiantang Estuary (after Lin, 2008). A highly distorted tidal front is abruptly raised several decimeters to several meters high to form tidal bores, which generally initiate at the middle ground of Ganpu (1) and DJS (2), peak at the between DQK (3) and YG (4), and disappear a little upstream of WY (8). Two photos taken near YG show a breaking tidal bore during a spring tide (left) and a undular tidal bore during a neap tide (right). Other stations include CQ (5), QB (6), ZK (7), FY (9), TL (10) and LCB (11).

maximum width of 2.5 km and a total area of 25 km^2 or more (Fan et al., 2012). Five short cores (WSG 1–5) were sampled from WSG intertidal flats, which is the largest intertidal flat along the south bank in the middle estuary. Two short cores (DQK1, 2) were taken from DQK tidal flat, a small pocket flat between two headlands with an area of ~500 m long and ~100 m wide, and a steep slope of 1/20. Only one short core (HJY) was collected from a narrow muddy flat near Zhapu, outside of the bore-affected reach (Fig. 1).

Sediment cores were split in half lengthwise in the laboratory, and the archived halves were sealed with preservative film and kept at the low-temperature (usually 4 °C) core repository. The sediment surface of the working halves was carefully scraped with a stainless steel knife to show clear sedimentary features on a flat plane (Figs. 3, 4). After detailed core logging, sediment samples were carefully extracted for grain-size analyses following strictly the rule that each analyzed sample should reflect a period of homogeneous sedimentation (Passega, 1964). Homogeneous sandy and muddy laminae were sampled separately on the basis of their shapes, paying full attention to avoid mixing heterolithic layers. For massive thick sandy beds, sampling spots were also constrained at a small patch with homogeneous compositions as far as possible (Fig. 4). In total, 395 sediment samples were collected with 105, and 290, from muddy and sandy (used here in a loose sense for sandy and silty laminae as compared to muddy laminae) layers, respectively.

Size-analyzed samples were weighed to 0.25–0.35 g for muddy deposits, and 0.45–0.55 g for sandy deposits. They were pretreated using the routine method at the State Key Laboratory of Marine Geology in Shanghai (Fan et al., 2006). Organic matter and carbonate were removed from the analyzed samples with 30% hydrogen peroxide and 10% diluted hydrochloric acid respectively. The sediment-suspension samples were repeatedly washed with deionized water until neutral, and then dispersed for a few minutes in an ultrasonic bath before

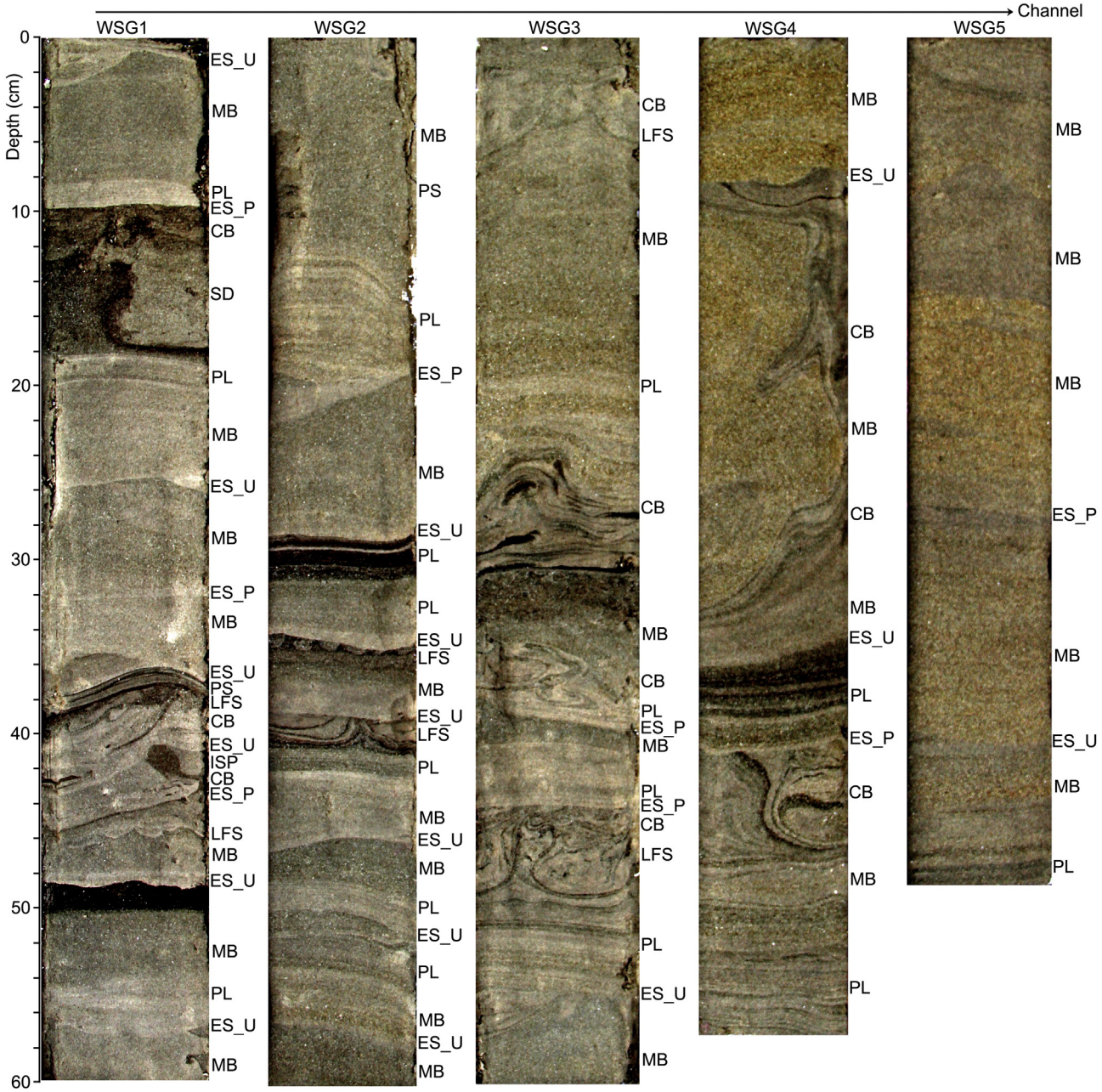

Fig. 3. Core photos of WSG1–5 show typical sedimentary structures produced by tidal bores and associated processes at the lower-middle tidal flats. ES: erosion surfaces, ES_P/U: planar/undular ES, MB: massive bedding, PL: parallel laminations, CB: convolute bedding, ISP: invasive sand patches, LFS: load-flame structures, PS: pipe-like structures, SD: sandy dikes.

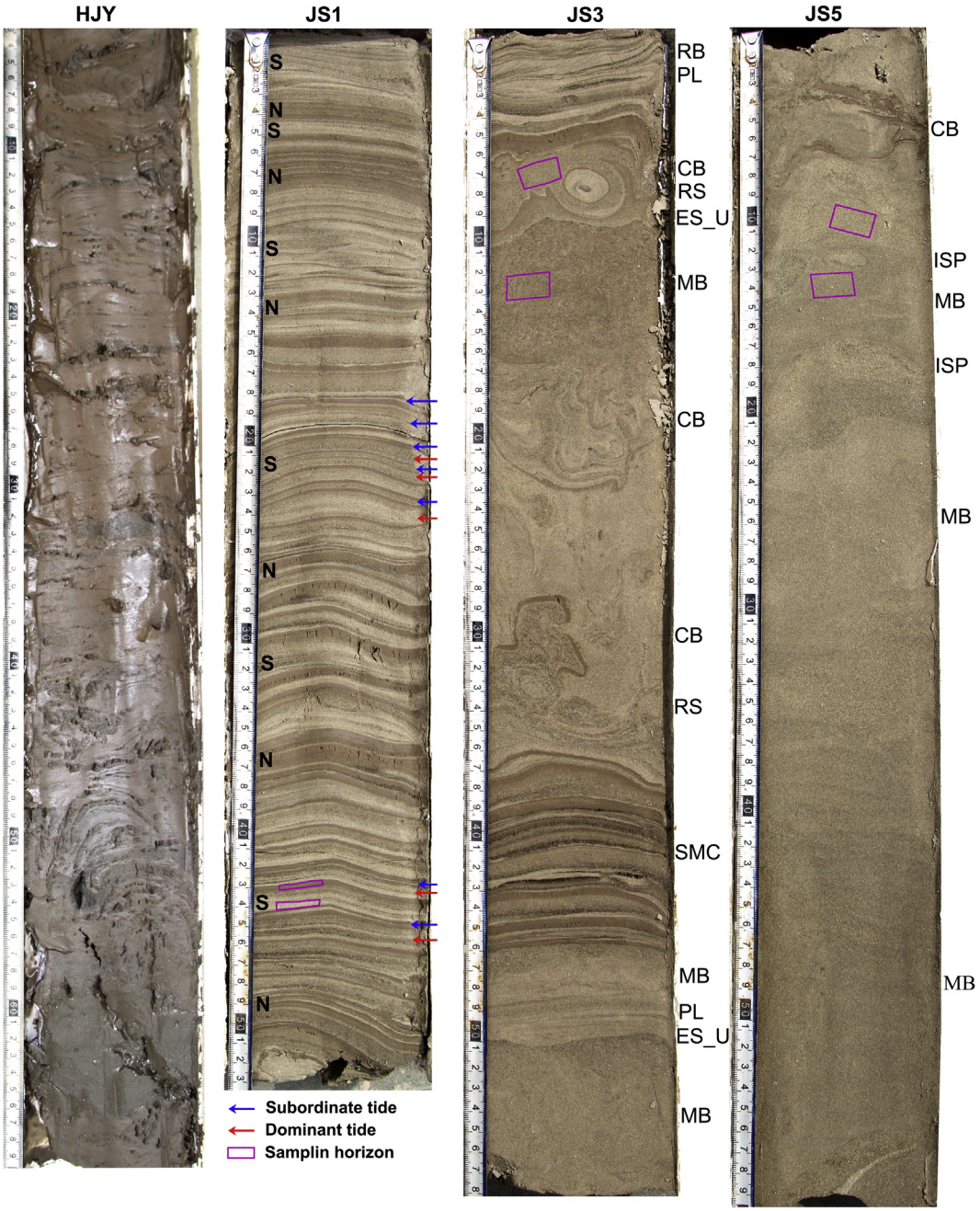

Fig. 4. Selected core photos show changes in sedimentary structures from massive beds of tidal-bore deposition (JS5) to tidal rhythmites (JS1), and then to heterolithic tidal deposits with faint bedding (HJY). N: neap tide, S: spring tide, ISP: irregular sand patches, RS: rolling structures, RB: ripple bedding (other acronyms are similar to those in Fig. 3).

measurement. The instrument used is a laser-diffracted size analyzer (Beckman Coulter LS230), with a detection range of 0.375–2000 μm.

3.2. Grain-size data analyses

Grain-size parameters were calculated through using moment methods (Friedman and Johnson, 1982), and log-normal functions were used to decompose grain-size distributions (GSDs) into dynamic populations (DPs) for genetic interpretation. GSDs of natural sediments are generally polymodal, and consist of more than one genetically meaningful dynamic sub-population (Weltje and Prins, 2007). Unmixing approaches to partition DPs includes end-member modeling and curve fitting methods. The curve fitting of GSDs compares them with specific mathematical functions, including the log-normal distribution (Shih and Komar, 1994), Weibull distribution (Sun et al., 2002), and log hyperbolic distribution (Bartholdy et al., 2007; Le Roux and Rojas, 2007). The Weibull and log hyperbolic distributions may simulate some typical sediment distributions (e.g. coarse unimodal fluvial sediments) better than the log-normal distribution (Kondolf and Adhikari, 2000; Hajek et al., 2010). However, comparison studies have not highlighted any particular advantage of these two complex distributions over the log-normal distribution method (Hill and McLaren, 2001; Barusseau, 2011), so log-normal functions were selected here.

In practice, the Curve Fitting tool of the Matlab program was used to partition GPDs. Most analyzed sediment samples have a quasi-unimodal size distribution, a principal mode plus a secondary mode at the finer or coarse side of the curve. So the number of partitioning groups was set to two, and the fitting magnitude was always high when examined by the Trust-Region algorithm. The Matlab-based Curve Fitting tool produced two sets of statistics for each case: (1) a

maximum multiple correlation coefficient (R^2) and a minimum root-mean-square error (RMSE), and (2) standard deviations and modes of the two log-normal-distribution subpopulations.

4. Results

4.1. Sedimentary structures

Both primary and secondary sedimentary structures are extensively and diversely developed in the bore-affected intertidal deposits (Figs. 3, 4). The most abundant structures in the transect of WSG1–5 are erosion surfaces (ES), massive bedding (MB), parallel laminations (PL), and convolute bedding (CB), with the common presence of load and flame structures (LFS) and scattered presence of pipe-like structures (PS), and invasive sand patches (ISP, Fig. 3). Erosion surfaces vary from straight to undular shapes. These structures are usually grouped into packages in an ascending way from ES, MB, PL, to CB. Each package is usually a few centimeters thick. Lateral variation in sedimentary structures is also obvious along the transect (Fig. 3). WSG5 near the main channel is characterized by well-developed massive bedding consisting of clean (light) yellow coarse sands or gray silty sands, and erosion surfaces are blurred. WSG3 and 4 have a distinguishing structural package within the transect, typically with archetypal parallel laminations and convolute bedding. WSG1 and 2 are characteristic of clear erosion boundaries, load and flame structures, and gray massive beds consisting of finer-grained deposits than their counterparts in WSG 4 and 5. Dark parallel laminae are mainly composed of organic debris and platy minerals.

Transect JS1–5 is characterized by a gradual shoreward transition from massive sands to heterolithic rhythmites (Fig. 4). JS5 is mainly composed of massive sands with two distorted muddy laminae at the top, and a close-up examination showed the abundance of irregular sandy patches (ISP) in massive sands. JS3 features alternations of two packages: thick sandy beds vs. thin heterolithic laminated beds. In the sandy packages sedimentary structures include ES, MB, PL, CB and rolling structures (RS), and heterolithic beds are composed of thin sand-mud couplets (SMC) with a few sandy laminae having graded bedding, ripple bedding (RB) and parallel laminations (Fig. 4). JS1 is characterized by regular alternations of thickening and thinning sand-laminae packages, denoting incomplete spring–neap tidal cycles. In the spring-tide (thicker) depositional packages, the thickness of the two consecutive sandy laminae sometimes varied conspicuously, denoting different energies of two semidiurnal tides in one day (diurnal inequality). JS2 is quite similar to JS1 but has much thicker sandy packages with some distorted bedding; JS4 looks like JS5 except it has more abundant convolute bedding. JS6–8 are closely similar to JS2, and DQK1 and 2 are comparable to JS4, with the exception that DQK1 has more irregular muddy laminae (not shown here).

HJY is characteristic of soft muddy deposits with high water content and faint bedding. Silts are present at the massive muddy layers in the form of thin (<2 mm) laminations or irregular patches without clear boundaries (Fig. 4).

4.2. Dynamic populations of grain-size distributions

Size data of 11 short cores from the north bank give a mean size range of 4.41–7.21 ϕ, mainly composed of fine sands and silts. Standard deviations vary from 1.32 ϕ to 1.85 ϕ, and reflect poor sorting (Cai et al., in press). Skewness and kurtosis values change within a range of 0.25 to 2.45 (fine skewed to very fine skewed) and 2.18 to 9.49 (mesokurtic to very leptokurtic). A general channel-ward coarsening trend along transect JS1–5 was observed with the depth-averaged mean size changing from 5.46 ϕ for JS1 to 4.78 ϕ for JS5, and sand components increasing from 5.87% (JS1) to 29.06% (JS5).

Size-frequency curves are mostly quasi unimodal distributions, usually having an elevated shoulder at the right (fine-grain) flank

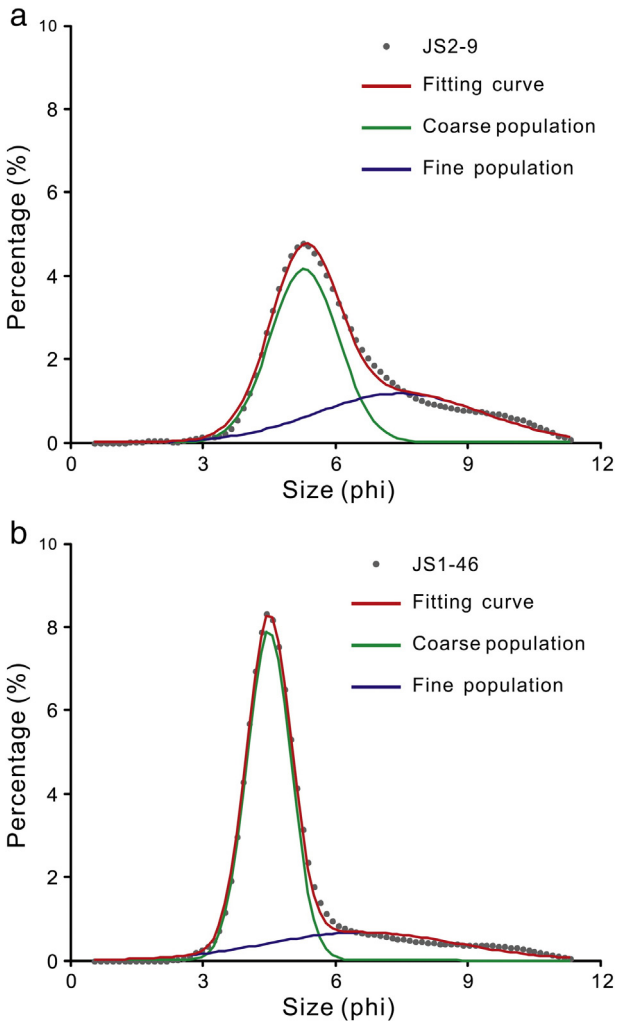

Fig. 5. Decomposition of grain size distributions into two log-normal curve components. Two samples, JS1-46 and JS2-29, were selected based on their mean and sorting values close to the average mean and sorting values of all sandy and muddy layers, respectively.

(Fig. 5). It is inferred that most of GSDs can be theoretically decomposed into two components reflecting different genetic processes. A log-normal curve-fitting function was selected to partition dynamic sub-populations using the following formula:

$$f(x) = E\left\{p_1[1/(\sigma_1\sqrt{(2\pi)}]\exp\left[-(x-m_1)^2/2{\sigma_1}^2\right] + (1-p_1)[1/(\sigma_2\sqrt{(2\pi)}]\exp\left[-(x-m_2)^2/2{\sigma_2}^2\right]\right\}$$

where E is a constant value of distribution density determined solely by interval of size class (0.1135 ϕ for the laser-diffracted size analyzer); p_1 and $(1 - p_1)$ are the percentages of the coarse and fine components based on their modal values. Parameters m_1, m_2, and σ_1, σ_2 are modal and sorting values of the two components in the log-normal distributions. All partitions were effectively examined with a higher mean value of 0.977 maximum multiple correlation coefficient (R^2).

The numerical partitioning results show that GSDs of sandy and muddy layers are composed of coarse and fine populations with obviously different proportions, and modal and sorting values (Fig. 6, Table 1). Sandy layers have coarser and better sorted coarse-populations than muddy layers. Mean modal and sorting values are 4.52 ϕ and 0.39 ϕ for the coarse populations of sandy layers, while they are 5.19 ϕ and 0.54 ϕ, respectively, for the muddy layers. The fine populations of sandy layers are generally coarser than those of muddy layers but with

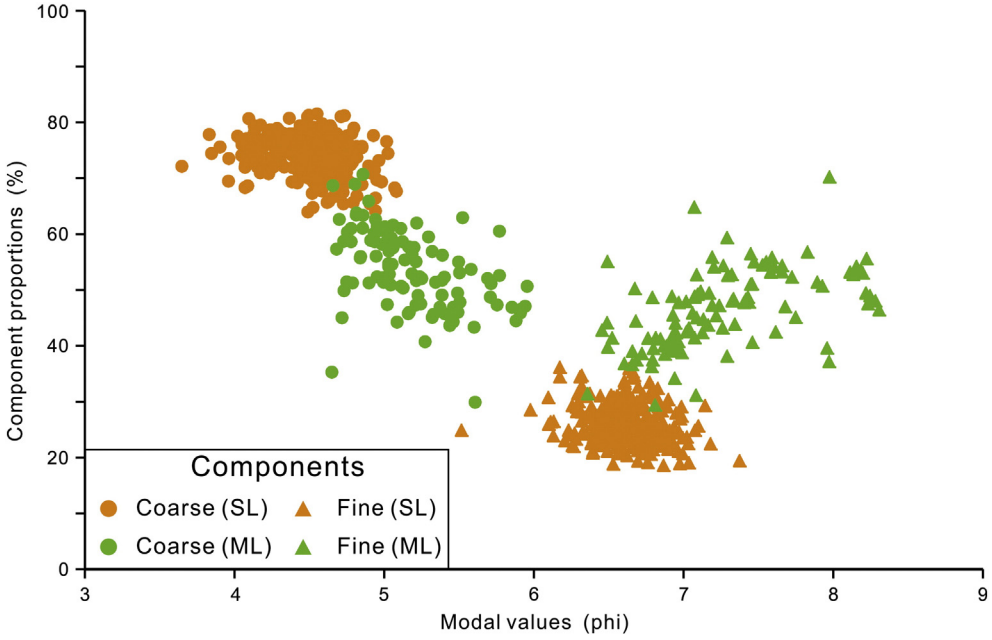

Fig. 6. Difference in modal values and proportions of coarse and fine components between sandy and muddy layers.

slightly poorer sorting. Mean modal size and sorting values are 6.63 ϕ and 1.71 ϕ for the fine populations of sandy layers, and 7.25 ϕ and 1.49 ϕ, respectively, for the muddy layers. Another major difference is that the predominance of coarse populations over fine populations is obvious in sandy layers with an average ratio of 74.02% over 25.98%, while it is weak for muddy layers with an average ratio of 53.6% over 46.40% (Fig. 6, Table 1). Most of these parametric differences are consistent with the general knowledge that sandy layers are deposited at higher energy environments than muddy layers.

5. Discussions

5.1. Depositional processes and products in the bore-affected estuarine reach

A few hydraulic data have been recently published, although it is very dangerous and difficult to gauge tidal bores (Han et al., 2003; Fan et al., 2012). Here we subdivided a semidiurnal tidal cycle at DQK into 7 stages using instrumental data (Fig. 7). The asymmetry between the flood and ebb tidal periods is obvious in the bore affected river section (Fig. 2), with a ratio of approximately 1:4 at DQK during a spring tide on May 1st, 2010 (Fig. 7). The maximum near-bottom (1 mab) current speeds were 2.1 and 0.7 m/s for the flood and ebb flows, respectively, with the former being 3 times the latter. The suspended sediment concentration (SSC) was highly elevated by the bore and subsequent rapid flow, reaching up to 1900 NTU (24.7 kg/m^3); while it was much less waked during the rapid ebbing stage, with a maximum SSC of ~550 NTU (7.15 kg/m^3). It is therefore extrapolated that tidal bores and flood currents play a major role in sediment-dynamic processes at the bore-affected river section, especially for the intertidal flats where the middle and upper parts have already been exposed during the occurrence of peak ebb currents in the main channel (Fig. 7; Fan et al., 2012).

Table 1
Statistics on parameters of coarse and fine populations of sandy and muddy layers.

Layer	Range	Coarse population			Fine population		
		Mode (ϕ)	Sorting (ϕ)	Proportion (%)	Mode (ϕ)	Sorting (ϕ)	Proportion (%)
Sandy	Minimum	3.65	0.33	63.86	5.52	1.10	18.57
	Maximum	5.09	0.56	81.43	7.38	2.27	36.14
	Average	4.52	0.39	74.02	6.63	1.71	25.98
Muddy	Minimum	4.66	0.37	29.81	6.36	1.34	29.41
	Maximum	5.96	1.01	70.59	8.31	1.83	70.19
	Average	5.19	0.54	53.60	7.25	1.49	46.40

The main channel in the river section from DJS to YG is generally very shallow, about 1–2 m deep during low tides (Han et al., 2003). The bore head in the section increases upstream from <1 m to over 2 m high during spring tides. The influence of bore passages is mainly limited to the main (secondary) channels and the lower part of the intertidal flat along the transect B-B′, while it extends to the middle intertidal flat along the A–A′ transect with a higher bore head (Fig. 8). The highly unstable wave front of tidal bores lasts only a few minutes (<2–3 min) with significant breakers and rollers, and it continues with a rapid but much more stable flow, lasting about 20 min. The continuous rising tide submerges the middle intertidal flat, potentially creating a supercritical flow regime over the shallow sandy flats with a peak depth-average speed of 2–3 m/s. Peak surface current speeds may reach up to 5–6 m/s for the advancing bores and subsequent rapid flows, in accordance with a bore celerity of 20–30 km/h (Pan and Huang, 2010). The rolling and shooting flows should induce significant erosion over the channel and submerged lower-middle tidal flats. It was observed that SSC was rapidly elevated from near zero to 1800 NTU during the first few minutes after the bore's arrival, and then remained above 1900 NTU with minor fluctuations (Fig. 7) during the residual stage. Extensive erosion surfaces in the core sediments were therefore attributed to such scouring processes by high energy flows, with the undular type mainly produced by bore rolling at the lower intertidal flats, and the planar type by rapid shooting flows at the middle intertidal flats (Figs. 3, 4, 8).

During the 2nd stage, the speed of rising tides is sharply decelerated, consequently resulting in rapid deposition. The data showed a sharp decrease in current speeds from >1.10 m/s to ~0.60 m/s over 30 min, accompanied with a much more rapid drop of SSC from ~1900 to ~450 NTU (Fig. 7). Rapid deposition can therefore produce massive sandy beds over erosion surfaces, and the critical flow regime accounts for well-developed parallel sandy laminations during the transition from supercritical to subcritical flows (Figs. 3, 4, 8). The grain size of sandy beds changing from coarse silts to fine sands is mainly linked with strengthening flow upstream from DJS to DQK, and from the

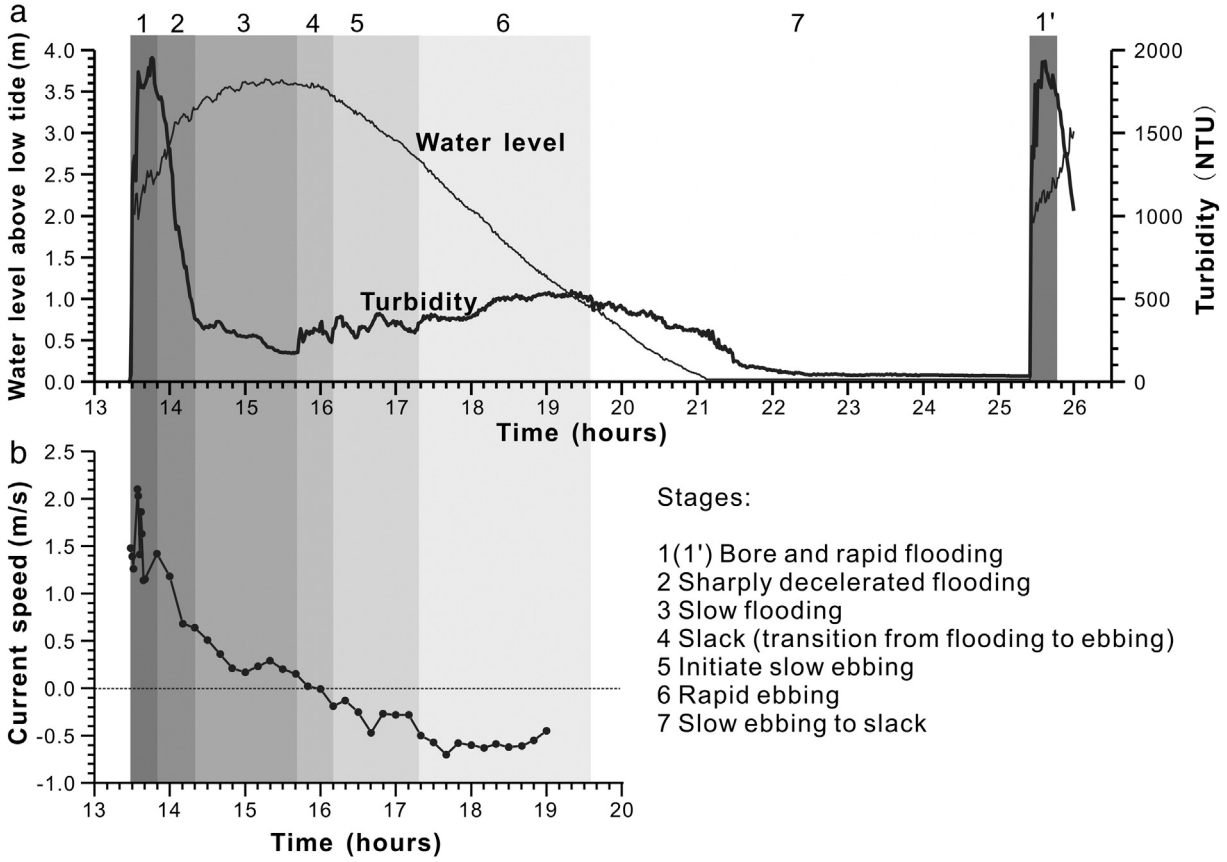

Fig. 7. Severn sub-stages of a spring tide in terms of different sediment-dynamic characteristics: (a) turbidity (bold line) vs. tidal level (hairline), and (b) current speeds. After Fan et al. (2012).

intertidal flat to the main channel (Fig. 8). However, a significant part of the observed parallel laminations are highly distorted into load and flame structures, convolute bedding, and flow rolls with water escape structures (Figs. 3, 4). Except for LFS, other soft-sediment deformation structures are conceivably produced by over-pressurization of water-saturated rapid deposition, because additional external stresses are expected with the abrupt increase in bore-water mass (about 1–3 m thick), the plunging action of bores, and the intense shear strength associated with rapid flows (Han et al., 2003; Donnelly and Chanson, 2005; Fan et al., 2012). Well-developed soft-sediment deformation structures attributed to the same mechanisms have been described in the bore-affected intertidal deposits at the Turnagain Arm (Alaska) and the Mont-Saint-Michel Bay (Tessier and Terwindt, 1994; Greb and Archer, 2007).

During the slow flooding and slack stages, the tide continues to rise to cover the upper intertidal flat (Figs. 7, 8). Weakening turbid flows promote deposition of fine grains to form silty and muddy laminae. JS1, from the upper part of DJS tidal flats, clearly shows heterolithic bedding with notable regular changes in both thickness and laminae color, denoting spring–neap tidal cycles. The package of thin and dark (due to higher muddy contents) laminated beds are considered to be neap tide deposits, while the thick, bright laminated beds are attributed to spring tides. Two successive silty laminae within the spring packages may show obviously different thicknesses (Fig. 4), which could result from significant asymmetry between the dominant and subordinate currents in a semidiurnal tide, or the pronounced diurnal inequality of dominant and subordinate tides in one day (Visser, 1980; Tessier and Gigot, 1989; Archer et al., 1995). In the above context, ebb currents have been extrapolated to contribute little coarse-grained deposition on the middle and upper intertidal flats where tidal rhythmites are developed (Fig. 7; Fan et al., 2012). Therefore, diurnal inequality of two successive tides should account for two neighboring thick–thin silty laminae (Fig. 4). The thickness and laminae numbers of each package of spring–neap tidal cycles decrease upward (Fig. 4), and are genetically linked to less frequent tidal flooding events because of rising elevation. Modern tidal rhythmites have been reported to develop primarily on the upper part of intertidal flats flanking main channels with tidal bores, including the Cobequid Bay–Salmon River Estuary (Dalrymple et al., 1991), the Mont-Saint-Michel Bay (Tessier, 1993), and the Turnagain Arm (Greb et al., 2011). This can be explained under two favorable conditions: (1) abundant source of fine-grained sediments resuspended from main channels by tidal bores and advected to tidal flats by flooding currents, and (2) highly protected environments from wave erosion in the inner estuaries.

5.2. Diagnostic sedimentary features of tidal-bore deposits

A tidal bore is a hydrodynamic shock as the tidal flow turns to rise, and its passage is very rapid, lasting only a few seconds to a few minutes (Chanson, 2012; Fan et al., 2012). High-energy tidal bores have little to do with deposition but are known as a destructive agent to induce significant erosion, sediment suspension and dispersion, and deformation of newly depositional strata. Intense erosion and sediment dispersion are continuous toward and throughout the subsequent rapid flooding period (Fig. 7). Most of the suspended sediments fall out immediately after the flow is halted to slow down quickly, and rapid deposition produces massive sandy beds, overlain with parallel laminated sands by the critical flow (Figs. 4, 8). The rapid depositional sediments, highly abundant with interstitial water, are likely to be deformed by the following tidal bores. Therefore, a general stratigraphical package formed by a series of genetically correlated processes is referred to here as a tidal-bore deposition. It consists of an erosion surface at the base, topped by massive sandy beds and parallel sandy laminations, which can be highly distorted by liquefaction to form convolute bedding, flow rolls, water

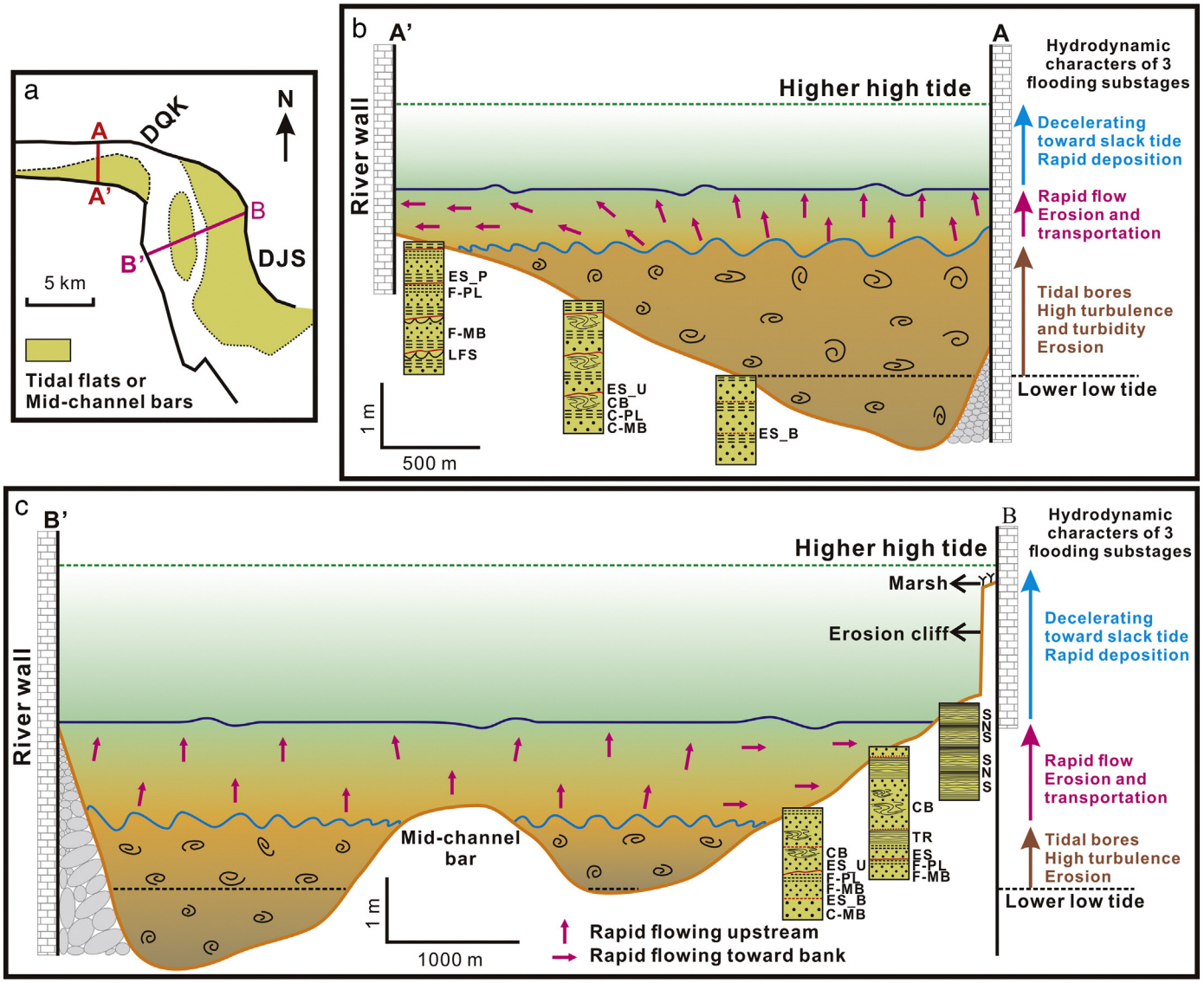

Fig. 8. Schematic models to show the genetic mechanism for typical tidal-bore deposits and tidal rhythmites, and their spatial distributions at the bore-affected river section. F- (C-) MB represents fine-grained (coarse-grained) massive bedding, F- (C-) PL represents fine-grained (coarse-grained) parallel laminations, and other acronyms are similar to those in Figs. 3, 4.

escape structures, load and flame structures, and irregular sandy rolling patches (Figs. 3, 4, 8).

Some diagnostic sedimentary features observed in the tidal-bore deposits from the Qiantang Estuary have also been reported in other bore-affected estuaries. For example, parallel sandy laminations were found to develop extensively on the UFR braided sand flats, with rapid flows and tidal bores in the Cobequid Bay–Salmon River Estuary (Dalrymple et al., 1991). Soft-sediment deformation structures are very well developed in the intertidal-flat deposits flanking the main channels with tidal bores in the Mont-Saint-Michel Bay (Tessier and Terwindt, 1994) and the Turnagain Arm (Greb and Archer, 2007). However, similar packages with erosion surfaces and massive sandy beds produced by high-energy tidal bores have never been reported in these estuaries. It can be ascribed to relatively small bores in the Cobequid Bay–Salmon River Estuary and the Mont-Saint-Michel Bay, but this is not true for the Turnagain Arm where tidal bores are generally very powerful, with breaking bores at spring tides (Greb and Archer, 2007). The reason for the latter case awaits further exploration.

The Late Jurassic Lourinhã Formation in the Lusitanian Basin (Portugal) is the first ancient example interpreted as a tidal-bore deposition (Martinius and Gowland, 2011). Such interpretation was based on three distinguishing characteristics: (1) erosion surfaces with a series of asymmetric and irregular excavations having short wave lengths and relatively high amplitudes, (2) overlain directly by homogeneous sandy beds, and (3) followed by low-angle parallel laminated sands to heterolithic laminae showing opposite dipping directions between the lower coarse-grained and the upper fine-grained sets. The depositional package mimics closely the modern tidal-bore deposition in the Qiantang Estuary in terms of extensive development of highly undular erosion surfaces, massive sandy beds and parallel sandy laminations (analog to low-angle foresets), and attests to its bore-genesis interpretation. There is some difference in the uppermost part of the modern and ancient tidal-bore depositional packages. These are mainly composed of soft-sediment deformation structures in the Qiantang Estuary, and low-angle bimodal cross-bedding sets in the Late Jurassic Lourinhã Formation. This difference can be ascribed to different interactions of tidal bores and tides with fluvial currents in the two bore-affected sections. Study transects are located at the lower bore-affected section of the Qiantang Estuary, where the bores are gradually accelerated to peak, so the bores and subsequent flood flows assume a predominant role over the ebb tide in shaping deposition. This results in highly distorted bedding by liquefaction and a lack of ebb tidal deposition because of the absence of weak current deposition, or a lack of preservation due to the strong erosion associated with tidal bores.

The formation of the Late Jurassic Lusitanian tidal-bore deposition was therefore extrapolated to an upstream part of the bore-affected river section, where decelerating tidal bores assumed a dominant role in deposition only in dry seasons (Martinius and Gowland, 2011), and increasing ebb currents potentially produced thick deposition to survive tidal-bore erosion.

Tidal bores may have occurred more extensively in the geological past because of the amplification of advancing tides into sea straits and epicontinental seas, and especially at periods with higher sea levels than present (Archer, 1998). Ancient tidal-bore deposits may therefore be extensively distributed, and attract increasing interest because of their potential as reservoirs of oil and gas (Martinius and Gowland, 2011). A high consistency of tidal-bore depositional characteristics on the basis of modern (Qiantang Estuary) and ancient (Lusitanian basin) sediments is exciting, and promises to stimulate research on the subject in terms of both theoretical and applied aspects.

5.3. Genetic interpretation of size parameters and sub-populations

Eleven short cores from the north bank of the Qiantang Estuary were analyzed for size composition to extract genetic information. Apparently homogeneous layers (by the naked eye) were sampled for size analyses in this study. Most of their GSDs are composed of one coarse (principal) and fine (secondary) component (Fig. 5). Each GSD was decomposed into two log-normal distribution components accordingly, with sandy and muddy laminae having completely different modes, sorting and proportional values (Table 1, Fig. 6). These are ascribed to different depositional processes on the tidal flats. Sandy laminae have a higher proportion (average of 74.02% vs. 53.60%) of relatively well sorted (a mean sorting value of 0.39 ϕ vs. 0.54 ϕ) coarse components than those of muddy laminae (Table 1, Fig. 6), conceivably resulting from their disparate depositional stages during waning flows or slack tides. The coarse components of both the sandy and muddy laminae are much better sorted than corresponding fine components. The good to very good sorting of coarse components is attributed to their settling mainly as single grains through selected deposition, while the poorly sorted fine components, with an average modal value less than 10 μm, deposit predominately as flocculants (Hsu and Liu, 2010; Fan, 2012; Law et al., 2013).

Flocculation is a major mechanism for fine particles to settle onto the seabed, including tidal flats, estuaries, shelves and deep oceans (Curran et al., 2004; Milligan et al., 2007; Hsu and Liu, 2010; Fan, 2012; Law et al., 2013). The floc fraction, numerically deduced by the inverse model of Curran et al. (2004), accounts for 35%–70% of the intertidal deposits in Willapa Bay (Law et al., in press). The floc fraction here was estimated in terms of percentages of fine components in the sediments. We did not observe a simple trend in floc fraction in the sandy laminae along the transect from JS1 to JS5 (Fig. 1). However, an increasing floc fraction trend was observed in the muddy laminae from 38.1% for JS3, through 43.25% for JS2, and up to 47.85% for JS1 (JS4 and JS5 excluded because of their predominance of sandy deposits). The increasing trend of the floc fraction with elevation is primarily related to waning energy from the channel to higher tidal flats. The highest floc fraction (50.87%) is present at HJY on the higher intertidal flat along the open bay region (Fig. 1), consistent with its sedimentary characters of soft massive muds with high water content and faint bedding (Fig. 4). The outer part of the central basin and the southeast bank of Hangzhou Bay also feature soft massive muds (Fan et al., 2005, 2012). The distribution pattern of the higher floc fraction in the lower Qiantang Estuary and Hangzhou Bay is therefore considered to be a link with relatively weak tidal energy and abundant fine-grained sediment source primarily from the downstream drift of the Yangtze River plume (Chen et al., 1990).

Based on typical sedimentary features, 197 sediment samples from five short cores JS1–JS5 were grouped into 36 TBDs (tidal-bore deposits), 119 TSDs (tidal sandy deposits) and 42 TMDs (tidal muddy deposits) according to their genetic interpretation. Three genetic groups have distinctly different distribution patterns in the bivariate diagrams (Fig. 9). It is easily understood that TMDs are finer and less sorted than sandy deposits (TBDs and TSDs), because TMDs are deposited during slack tides with abundant flocs. Why TMDs have the lowest skewness values is possibly due to the close proportions of two subpopulations. A mixture of two log-normal subpopulations with similar or close proportions will create a broad but close to symmetrical size distribution (Fig. 5a). The asymmetry of size distributions increases as the difference in ratios of two mixing subpopulations increases. Sandy laminae tend to have higher skewness values because their GSDs take the main shape of principal subpopulations but with a significant tail produced by admixture of secondary subpopulations (Fig. 5b).

Sandy layers can be produced by tidal bores and ordinary tidal currents. TBDs have coarser and less sorted GSDs than TSDs (Fig. 9a), because TBDs are a product of rapid deposition after energetic tidal bores and subsequent rapid flows in the main channel and on the

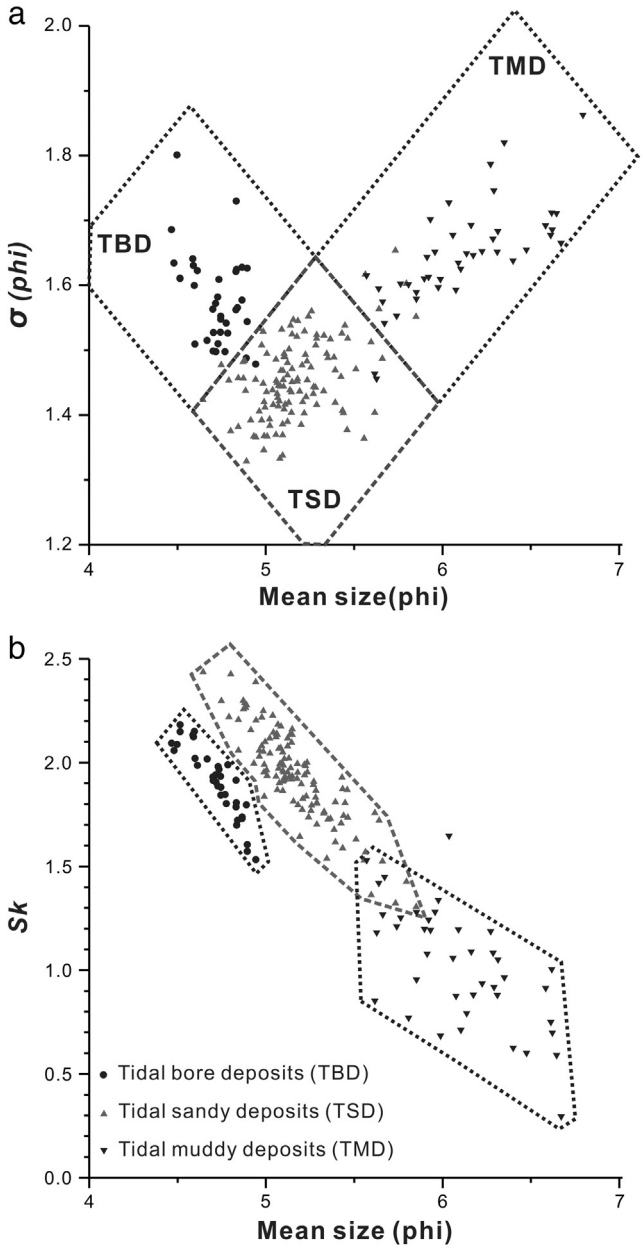

Fig. 9. Bivariate plotting of size parameters potentially served as an important tool to discriminate tidal-bore deposits from other deposits in the estuaries, (a) mean size vs. sorting, (b) mean size vs. sknewness.
After Fan et al. (2012).

adjacent lower tidal flats. TSDs are deposited by ordinary tidal flows on the middle and upper tidal flats through selective transport and sedimentation processes that operate over prolonged periods and distances, producing finer but better sorted deposits. Skewness values of TBDs overlap with those of TSDs, showing narrower distribution ranges and smaller average values.

Bivariate plots of sorting and skewness parameters, or sorting and kurtosis parameters, also demonstrate the different distribution patterns of TBDs, TSDs and TMDs (Fan et al., 2012). In a word, bivariate plotting of any two size parameters can be used as a powerful method to discriminate tidal-bore deposits from other ordinary tidal deposits. The bivariate plotting method has been widely used to explore clues to depositional modes and sedimentary environments since it was elaborately discussed by Folk and Ward (1957). For example, the method was successfully employed by Friedman (1967) to discriminate between river and beach sands. However, bivariate plots may fail in discriminating dynamic environments in case of multimodal size distributions. No trend variations were found in the parametric relationships of beach sands among different compartments or morphodynamic zones along the northern coast of the Gulf of Lions (Barusseau, 2011). Success in our case study may be linked to the strict sampling strategy adopted, using only individual sedimentary units that represent single homogeneous sedimentation processes. A strict sampling methodology is therefore stressed, in order to succeed in discriminating depositional environments associated with tidal bores from other estuarine processes.

5.4. Sedimentary facies model of the Qiantang Estuary

The incised-valley fill sequences and development of the Qiantang Estuary have been well studied on the basis of hundreds of core stratigraphic data (Zhang and Li, 1996; Lin et al., 2005; Li et al., 2006). Maximum transgression was extropolated to occur in the period of 7500–6000 yr B.P., when Hangzhou Bay reached its maximum extent (Zhang and Li, 1996). Since then the Hangzhou Bay–Qiantang Estuary has undergone significant morphologic changes because of accretion at both the basin and estuary. The maximum thickness of estuarine facies reaches up to 20 m, and the bay is generally quite shallow with a mean water depth of ~10 m during low tides (Zhang and Li, 1996). Due to the Coriolis effect, flooding currents converge toward the north bank to strengthen flow and produce erosion, while ebbing currents diverge out of the bay and are deflected to the south bank and induce accretion. Along the Jinshan transect, the north bank (south bank) have retreated (prograded) 20–30 km since 6000 yr B.P., and the bay head has moved downstream over 50 km. The most significant shoreline change occurred in the last three centuries owing to land reclamation and waterway management (Han et al., 2003). Morphological evolution in the past 300 years and sediment distribution patterns in the estuary are discussed next, to extract a general sedimentary facies model for the bore-affected estuary (Fig. 10).

The outer part of Hangzhou Bay (western boundary near Jinshan, Fig. 10) is very flat and quite shallow with an average depth of 8–10 m during low tide. Surface sediments are predominantly composed of clayey silts and muds. These fine-grained sediments are primarily sourced from the Yangtze River plume through alongshore currents and tidal flows, so the outer part of the bay is also considered a part of subaqueous Yangtze Delta (ECCHE, 1992; Zhang and Li, 1996; Li et al., 2006).

The inner part of Hangzhou Bay extends over 70 km from a few kilometers east of Jinshan to a few kilometers west of Ganpu (Fig. 10). It is characterized by extensive development of erosion troughs and accretion ridges over silty ground (Fig. 10). The mechanism to develop erosion troughs is spatially varied. Two series of bank-parallel deep

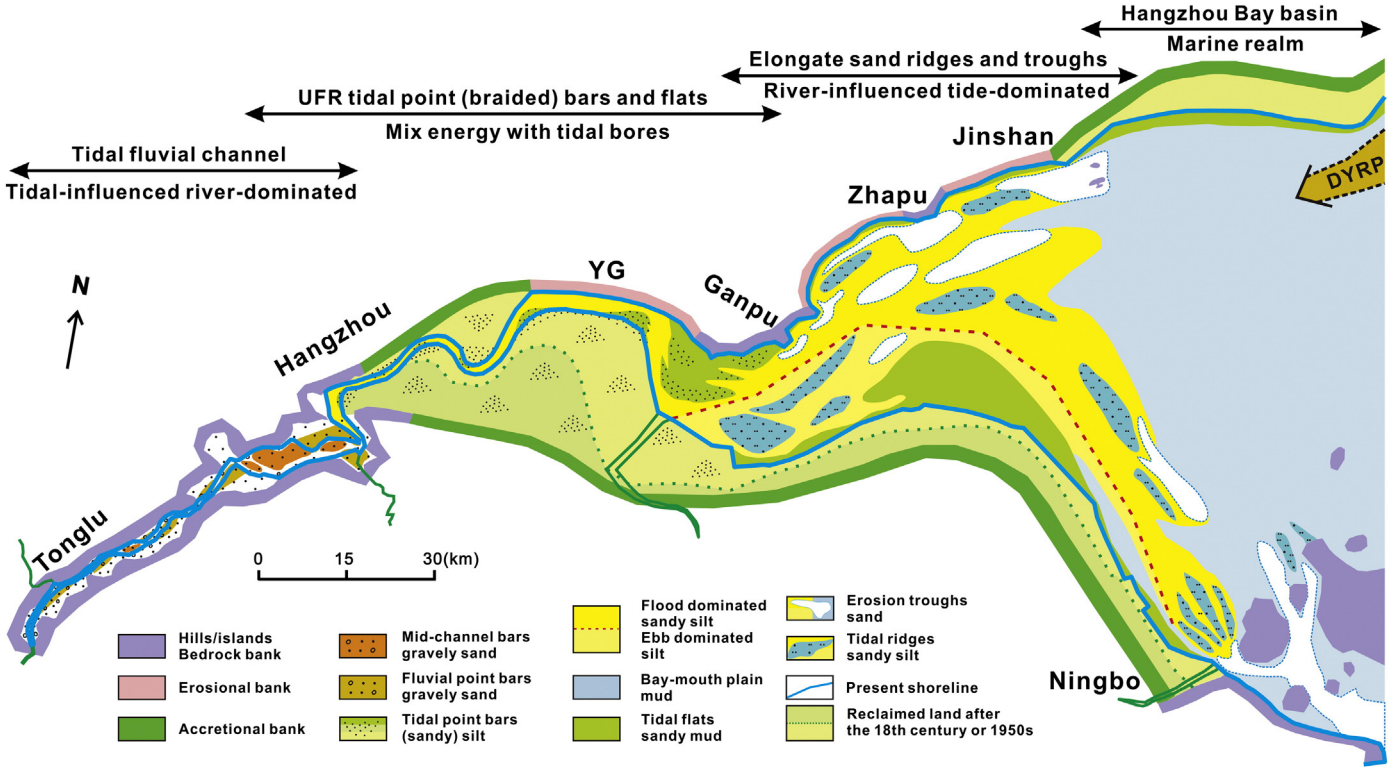

Fig. 10. A sedimentary facies model of a hypertidal estuary with energetic tidal bores and abundant sediment supply, formulated based on the Hangzhou Bay–Qiantang Estuary. The upper estuary is a tide-influenced fluvial dominated section with coarsest sediments (sandy gravel to gravely sand), characterized by a relatively straight main channel with fluvial point bars and mid-channel bars. The middle estuary is a bore-affected section with finest sediments (coarse silts to fine sands), featuring a highly sinuous channel with tidal point bars. The outer estuary is a marine-dominated section, whose north part is flood-dominated with well-developed linear sand troughs and ridges, while the south part is ebb-dominated with an extensive distribution of muddy flats and a few ridges. The marine basin (outer part of Hangzhou Bay) receives a huge amount of fine-grained sediments from the downstream drift of the Yangtze River plume (DYRP), also considered as an important part of the Yangtze subaqueous delta.

troughs are mainly produced by strengthening flooding currents due to a convergent effect and are concentrated near some rocky islands. For example, the erosion trough off the Jinshan cape is 30–40 m deep on average with a maximum depth of 51 m, and ~2 km wide, extending 11.3 km long. The western end of the Jinshan deep trough is followed by accretion ridges, a few meters above the surrounding ground (ECCHE, 1992; Xie et al., 2009). Deep troughs between any two rocky islands are very well developed at the southeastern area with an erosion depth up to a few tens of meters, and scouring materials accumulate at the northwestern ends of the troughs or islands to form sandy ridges. Erosion troughs are generally covered by coarse sands, while accretion ridges are mainly composed of sandy silts (Fig. 10). The western and southern parts of the bay are dominated by ebb currents, much weaker than flood currents, favoring fine-grained sediment accumulation, so the south bank undergoes continuous accretion with extensive muddy intertidal flats (Figs. 1, 10; Fan et al., 2005). However, ebb flows are relatively forceful at the bay head, producing sand bars and ridges at the southwestern part of the bay head (opposite to Ganpu), shallow erosion channels (barb-like, see Dalrymple et al. (2012) for a definition) on the western flank of the muddy intertidal flat, and small and shallow erosion troughs at the front of the muddy flat (Fig. 10). The morpho- and sediment-dynamic settings of the section is comparable with those of the outer Severn Estuary (Harris, 1988; Allen, 1990; Wells, 1995), and zone 1 of the Cobequid Bay–Salmon River Estuary with elongate sand bars (ridges) separated by erosion troughs (Dalrymple et al., 1991, 2012). The difference is that the southern flank of Hangzhou Bay has developed extensive muddy flats from ebb domination as a result of the huge sediment supply from the Yangtze River plume.

The middle estuary presently occupies a winding channel with tidal bores, extending nearly 100 km, from a few km east of DJS to WY (Figs. 2, 10). The main channel is predominantly composed of coarse silts to fine sands. They are flanked by tidal flats along the outer bends, also known as estuarine point-bars (Allen, 1991; Wells, 1995) or tidal point-bars (Dalrymple and Choi, 2007). The lower flats are usually extensively developed with flood barbs at the seaward end, while the higher flats and marshlands are absent or quite limited in extent with cascading terraces and cliffs. There is a general fining trend of sediments from the main channel toward the bank. The main channel and the lower intertidal flats are dominated by tidal-bore deposition (see Section 5.2 for detailed characteristics), and the upper intertidal flats and marshlands are characterized by rhythmic deposition, potentially recording spring–neap cycles or seasonal cycles. The depositional zone in between features alternative depositional units of tidal bores and ordinary tides. The present main channel is very narrow with a width varying from a few hundred meters to 2–3 km, although it was very wide before large scale land reclamation during the past three centuries. The full-water bank width of the channel was 20–30 km in the 18th century. The wide channel was occupied by extensive braided sand bars and flats, which were highly mobile because of active shifting of the main channel (Chen et al., 1990; Han et al., 2003; Yu et al., 2012), very similar to zone 2 of the Cobequid Bay–Salmon River Estuary termed as UFR braided sand flats (Dalrymple et al., 1991). Most of the mobile braided sand bars and flats have been reclaimed during the past 300 years, and the man-made channel follows a meandering form, which characterizes the middle (mixed-energy) part of tide-dominated estuaries in the facies model of Dalrymple et al. (1992).

The upper estuary extends over 80 km from WY to LCB. It is river dominated with a tidal influence (Figs. 2, 10). The sinuousness of the channel is much lower than that of the middle estuary, and the channel is quite stable. Surface sediments in the main channel are dominated by sandy gravels, and those of fluvial point-bars and mid-channel bars are mainly composed of gravelly sands (Zhang and Li, 1996; Han et al., 2003; Fan et al., 2012).

In summary, tripartite facies divisions are distinct in the Qiantang Estuary, and their sedimentary features are highly analogous to the well-known tide-dominated estuarine facies model based on the Cobequid Bay–Salmon River Estuary (Dalrymple et al., 1991, 1992). The main channel shows a similar coarse-fine-coarse pattern of sediment size and a low-high-low pattern of sinuosity from the outer marine-dominated, through the middle mixed-energy, to the inner river-dominated estuary. However, the outer Qiantang estuary has obviously different morphodynamic features between the north and south parts due to a Coriolis-force effect that is remarkably magnified in the embayment. The middle Qiantang estuary features intense bore action and rapid filling processes, the latter due to abundant sediment supply both from the Qiantang and Cao'e rivers (6.58×10^6 and 1.28×10^6 tons/yr, respectively) and the sea. The latter is sourced from erosion of the sea bank and bottom, typically the north part of the basin, and the downstream drift of the Yangtze River plume (DYRP) that is estimated to reach up to 0.48×10^8 tons/yr, a magnitude higher than sediment input from the Qiantang River (ECCHE, 1992). The Qiantang Estuary is therefore referred as a sediment-rich progradational estuary in contrast to other sediment-deficit transgressive or early-regressive estuaries (Li et al., 2006; Tessier, 2012).

6. Conclusions

The Qiantang Estuary is home to the world's largest tidal bore with a peak bore head of 2–3 m high. Undular bores are usually formed during neap tides, gradually growing toward intense breaking bores during spring tides with a maximum flood velocity of over 5 m/s. The rolling tidal bores and subsequent shooting flood flows are destructive forces that produce new-strata deformation and sediment erosion and dispersion. Most of the resuspended sediments settle down rapidly in the following stage of sharply decelerating flooding flows. All three successive processes last for less than one hour and are genetically correlated, so the product of intense erosion and rapid deposition is collectively termed as tidal-bore deposits (TBDs) in this study.

Typical depositional packages of tidal bores and associated tidal flows are characterized by (1) the presence of an undular (planar) erosion surface at the base, produced by rolling bores or fast shooting flows, (2) overlying massive or homogeneous sandy beds resulting from rapid deposition of sharply decelerated flows, (3) parallel laminated sandy beds representing critical flows and heterolithic beds representing waning flows, and (4) abundant soft-sediment deformation structures including convolute bedding, flames, boiled sand patches and water-escaped structures, in the newly depositional units. Bivariate plotting of size parameters is an important tool to distinguish TBDs from tidal sandy and muddy deposits, especially for sandy beds whose origins may be unclear from structural criteria alone. In general, TBDs have coarser and less sorted grain-size distributions (GSDs) than tidal sandy deposits (TSDs), because TBDs are a product of rapid deposition at or near the main channel following the highly energetic mixing process of tidal bores, while TSDs are formed by ordinary tidal currents on higher intertidal flats through selective transport and deposition over prolonged distances and periods.

Characteristic tidal-bore deposition is primarily distributed along the main channel and the adjacent lower tidal flat. It gradually transits shoreward into alternations of TBDs and heterolithic beds at the middle tidal flat, toward tidal rhythmites at the higher tidal flat. Tidal rhythmites may display tidal periods of diurnal inequality and incomplete spring–neap cycles, or seasonal flood–dry cycles. Along the axis, tidal-bore deposits at the middle estuary are finest (coarse silts to fine sands) in comparison with the upper and outer estuarine deposits, which are composed of sandy gravels to gravely sands and coarse sands to sandy silts, respectively. Tripartite estuarine facies divisions closely mimic well-known tide-dominated estuarine facies models, except well-developed tidal-bore deposition at the middle estuary, and the obvious different depositional patterns between the northern and southern part of the outer estuary. The northern part is characteristic of well-developed linear erosion troughs and accretion ridges with coarser deposits produced by stronger flood currents, while the

southern part features extensive muddy bank development, with a few linear ridges and shallow scouring troughs from relatively weaker ebb currents.

Acknowledgments

This work is supported by the National Natural Science Foundation of China (NSFC) under Grant Numbers 41076016 and 41276045, and the Fundamental Research Funds for the Central University, and the China Geological Survey (GZH201100203). We wish to thank Yijing Wu and Lingling Chen for their assistance in fieldtrips and laboratory work. Appreciation also goes to Prof. J.T. Wells and two anonymous reviewers for constructive suggestions on previous versions. The authors are grateful to Dr. G.S. Burr (University of Arizona) for checking the English presentation.

References

Allen, J.R.L., 1990. The Severn Estuary in southwest Britain: its retreat under marine transgression, and fine-sediment regime. Sediment. Geol. 66, 13–28.
Allen, G.P., 1991. Sedimentary processes and facies in the Gironde estuary: a recent model for macrotidal estuarine systems. In: Smith, D.G., Reinson, G.E., Zaitlin, B.A., Rahmani, R.A. (Eds.), Clastic Tidal Sedimentology. Can. Soc. Petrol. Geol. Mem., 16, pp. 29–40 (Calgary).
Allen, G.P., Posamentier, H.W., 1993. Sequence stratigraphy and facies model of an incised valley fill: the Gironde Estuary, France. J. Sediment. Petrol. 63, 378–391.
Archer, A.W., 1998. Hierarchy of controls on cyclic rhythmite deposition: carboniferous basins of eastern and mid-continental, USA. In: Alexander, C.R., Davis Jr., R.A., Henry, V.J. (Eds.), Tidalites: Processes and Products. SEPM, Tulsa, pp. 59–68.
Archer, A.W., 2013. World's highest tides: hypertidal coastal systems in North America, South America and Europe. Sediment. Geol. 284–285, 1–25.
Archer, A.W., Kuecher, G.J., Kvale, E.P., 1995. The role of tidal-velocity asymmetries in the deposition of silty tidal rhythmites (Carboniferous, Eastern Interior Coal Basin, U.S.A.). J. Sediment. Res. 65, 408–416.
Bartholdy, J., Christiansen, C., Pedersen, J.B.T., 2007. Comparing spatial grain-size trends inferred from textural parameters using percentile statistical parameters and those based on the log-hyperbolic method. Sediment. Geol. 202, 436–452.
Bartsch-Winkler, S., Lynch, D.K., 1988. Catalog of worldwide tidal bore occurrences and characteristics. US Geol. Surv. Circ. No. 1022. (17 pp.).
Barusseau, J.P., 2011. Influence of mixtures of grain-size populations on the parametric and modal characteristics of coastal sands (Hérault, Mediterranean Sea, France). J. Sediment. Res. 81, 611–629.
Cai, G.F., Fan, D.D., Shang, S., Wu, Y.J., Shao, L., 2013. Difference in grain-size parameters of tidal deposits derived from the graphic and moment methods and its potential causes. Mar. Geol. Quat. Geol. (in press in Chinese with an English abstract).
Chanson, H., 2009. Current knowledge in hydraulic jumps and related phenomena: a survey of experimental results. Eur. J. Mech. A. Solids 28, 191–210.
Chanson, H., 2012. Tidal Bores, Aegir, Eagre, Mascaret, Pororoca: Theory and Observations. World Scientific, Singapore (200 pp.).
Chanson, H., Reungoat, D., Simon, B., Lubi, P., 2011. High-frequency turbulence and suspended sediment concentration measurements in the Garonne River tidal bore. Estuar. Coast. Shelf Sci. 95, 298–306.
Chen, J., Liu, C., Zhang, C., Walker, H.J., 1990. Geomorphological development and sedimentation in the Qiantang Estuary and Hangzhou Bay. J. Coast. Res. 6, 559–572.
Curran, K.J., Hill, P.S., Schell, T.M., Milligan, T.G., Piper, D.J.W., 2004. Inferring the mass fraction of floc-deposited mud: application to fine-grained turbidites. Sedimentology 51, 927–944.
Dai, Z.H., Zhou, C.S., 1987. The Qiantang bore. Int. J. Sediment Res. (1), 125–133.
Dalrymple, R.W., Choi, K.S., 2007. Morphologic and facies trends through the fluvial-marine transition in tide-dominated depositional systems: a systematic framework for environmental and sequence-stratigraphic interpretation. Earth Sci. Rev. 81, 135–174.
Dalrymple, R.W., Knight, R.J., Zaitlin, B.A., Middleton, G.V., 1990. Dynamics and facies model of a macrotidal sand bar complex. Sedimentology 35, 577–612.
Dalrymple, R.W., Makino, Y., Zaitlin, B.A., 1991. Temporal and spatial patterns of rhythmite deposition on mud flats in the macrotidal Cobequid Bay–Salmon River estuary, Bay of Fundy, Canada. In: Smith, D.G., Reinson, G.E., Zaitlin, B.A., Rahmani, R.A. (Eds.), Clastic Tidal Sedimentology. Can. Soc. Petrol. Geol. Mem, 16, pp. 137–160.
Dalrymple, R.W., Zaitlin, B.A., Royd, R., 1992. Estuarine facies models: conceptual basis and stratigraphic implications. J. Sediment. Petrol. 62, 1130–1146.
Dalrymple, R.W., Mackay, D.A., Ichaso, A.A., Choi, K.S., 2012. Processes, morphodynamics, and facies of tide-dominated estuaries. In: Davis Jr., R.A., Dalrymple, R.W. (Eds.), Principles of Tidal Sedimentology. Springer, London, pp. 79–107.
Donnelly, C., Chanson, H., 2005. Environmental impacts of undular tidal bores in tropical rivers. Environ. Fluid Mech. 5, 481–494.
ECCHE (Editorial Committee for Chinese Harbors and Embayments), 1992. Chinese Harbors and Embayments (Part V). China Ocean Press, Beijing (357 pp (in Chinese)).
Fan, D.D., 2012. Open-coast tidal flats. In: Davis Jr., R.A., Dalrymple, R.W. (Eds.), Principles of Tidal Sedimentology. Springer, London, pp. 187–229.
Fan, D.D., Guo, Y.X., Li, C.X., Yuan, L.H., 2005. Grain-size distributions and their applications on Andong intertidal facies analyses in the Hangzhou Bay. J. Tongji Univ. (Nat. Sci.) 33, 687–691 (in Chinese with English abstract).
Fan, D.D., Guo, Y.X., Wang, P., Shi, Z., 2006. Cross-shore variations in morphodynamic processes of an open-coast mudflat in the Changjiang Delta: with an emphasis on storm impacts. Cont. Shelf Res. 26, 517–538.
Fan, D.D., Cai, G.F., Shang, S., Wu, Y.J., Zhang, Y.W., Gao, L., 2012. Sedimentation processes and sedimentary characteristics of tidal bores along the north bank of the Qiantang Estuary. Chin. Sci. Bull. 57, 1157–1167.
Folk, R.L., Ward, W.C., 1957. Brazos River bar: a study in the significance of grain size parameters. J. Sediment. Petrol. 27, 3–26.
Friedman, G.M., 1967. Dynamic processes and statistical parameters compared for size frequency distributions of beach and river sands. J. Sediment. Petrol. 37, 327–354.
Friedman, G.M., Johnson, K.G., 1982. Exercises in Sedimentology. John Wiley Sons, New York (208 pp.).
Greb, S.F., Archer, A.W., 2007. Soft-sediment deformation produced by tides in a meizoseismic area, Turnagain Arm, Alaska. Geology 35, 425–438.
Greb, S.F., Archer, A.W., Debore, D.G., 2011. Apogean–perigean signals encoded in tidal flats at the fluvio-estuarine transition of Glacier Creek, Turnagain Arm, Alaska: implications for ancient tidal rhythmites. Sedimentology 58, 1434–1452.
Hajek, E.A., Huzurbazar, S.V., Mohrig, D., Lynds, R.M., Heller, P.L., 2010. Statistical characterization of grain-size distributions in sandy fluvial systems. J. Sediment. Res. 80, 184–192.
Han, Z.C., Dai, Z.H., Li, G.B., 2003. Regulation and Exploitation of Qiantang River Estuary. China Water Publication, Beijing (554 pp (in Chinese with English abstract)).
Harris, P.T., 1988. Large-scale bedforms as indicators of mutually evasive sand transport and the sequential infilling of wide-mouthed estuaries. Sediment. Geol. 57, 273–298.
Hill, S.H., McLaren, P., 2001. A comparison between log-hyperbolic and model-independent grain-size distribution in sediment trend analysis. J. Coast. Res. 17, 931–935.
Hsu, R.T., Liu, J.T., 2010. In-situ estimations of the density and porosity of flocs of varying sizes in a submarine canyon. Mar. Geol. 276, 105–109.
Koch, C., Chanson, H., 2008. Turbulent mixing beneath an undular bore front. J. Coast. Res. 24, 999–1007.
Kondolf, G.M., Adhikari, A., 2000. Weibull vs. log-normal distributions for fluvial gravels. J. Sediment. Res. 70, 456–460.
Law, B.A., Milligan, T.G., Hill, P.S., Newgard, J., Wheatcroft, R.A., Wiberg, P.L., 2013. Flocculation on a muddy intertidal flat in Willapa Bay, Washington, Part I: a regional survey of the grain size of surficial sediments. Cont. Shelf Res. 60S, S136–S144.
Le Roux, J.P., Rojas, E.M., 2007. Sediment transport patterns determined from grain size parameters: overview and state of the art. Sediment. Geol. 202, 473–488.
Li, C.X., Wang, P., Fan, D.D., Yang, S., 2006. In: Dalrymple, R.W., Leckie, D.A., Tillman, R.W. (Eds.), Characteristics and formation of late Quaternary incised-valley-fill sequences in sediment-rich deltas and estuaries: case studies from China. Incised Valleys in Time and Space, 85. SEPM Special Publications, Tulsa, pp. 141–160.
Lin, B.Y., 2008. Characters of Qiantang Bore. Chinese Ocean Press, Beijing (212 pp (in Chinese)).
Lin, C.M., Zhuo, H.C., Gao, S., 2005. Sedimentary facies and evolution in the Qiantang River incised valley, eastern China. Mar. Geol. 219, 235–259.
Lubin, P., Glockner, S., Chanson, H., 2010. Numerical simulation of a weak breaking tidal bore. Mech. Res. Commun. 37, 119–121.
Madsen, P.A., Simonsen, H.J., Pan, C.H., 2005. Numerical simulation of tidal bores and hydraulic jumps. Coast. Eng. 52, 409–433.
Martinius, A.W., Gowland, S., 2011. Tide-influenced fluvial bedforms and tidal bore deposits (Late Jurassic Lourinhã Formation, Lusitanian Basin, Western Portugal). Sedimentology 58, 285–324.
Milligan, T.G., Hill, P.S., Law, B.A., 2007. Flocculation and the loss of sediment from river plumes. Cont. Shelf Res. 27, 309–321.
Pan, C., Huang, W., 2010. Numerical modeling of suspended sediment transport affected by tidal bore in Qiantang Estuary. J. Coast. Res. 26, 1123–1132.
Pan, C.H., Lin, B.Y., Mao, X.Z., 2007. Case study: numerical modeling of the tidal bore on the Qiantang River, China. J. Hydraul. Eng. 133 (2), 130–138.
Passega, R., 1964. Grain size representation by CM patterns as a geological tool. J. Sediment. Petrol. 3, 830–847.
Shih, S.M., Komar, P.D., 1994. Sediments, beach morphology and sea cliff erosion within an Oregon coast littoral cell. J. Coast. Res. 10, 144–157.
Simpson, J.H., Fisher, N.R., Wiles, P., 2004. Reynolds stress and TKE production in an estuary with a tidal bore. Estuar. Coast. Shelf Sci. 60, 619–627.
Sun, D.H., Bloemendal, J., Rea, D.K., Vandenberghe, J., Jiang, F.C., An, Z.S., Su, R.X., 2002. Grain-size distribution function of polymodal sediments in hydraulic and aeolian environments, and numerical partitioning of the sedimentary components. Sedimentology 152, 263–277.
Tessier, B., 1993. Upper intertidal rhythmites in the Mont-Saint-Michel Bay (NW France): perspectives for paleoreconstruction. Mar. Geol. 110, 355–367.
Tessier, B., 2012. Stratigraphy of tide-dominated estuaries. In: Davis, R.A., Dalrymple, R.W. (Eds.), Principles of Tidal Sedimentology. Springer, London, pp. 109–128.
Tessier, B., Gigot, P., 1989. A vertical record of different tidal cyclicities: an example from the Miocene marine molasses of Digne (Haute Provence, France). Sedimentology 36, 767–776.
Tessier, B., Terwindt, J.H.H., 1994. An example of soft-sediment deformations in an intertidal environment: the effect of tidal bores. C. R. Acad. Sci. 319, 217–223 (in France with English abstract).
Visser, M.J., 1980. Neap–spring cycles reflected in Holocene subtidal large-scale bedform deposits: a preliminary note. Geology 8, 543–546.

Wells, J.T., 1995. Tide-dominated estuaries and tidal rivers. In: Perillo, G.M.E. (Ed.), Geomorphology and Sedimentology of Estuaries. Developments in Sedimentology, 53. Elsevier, Amsterdam, pp. 179–205.
Weltje, G.J., Prins, M.A., 2007. Genetically meaningful decomposition of grain-size distributions. Sediment. Geol. 202, 409–424.
Wolanski, E., Moore, K., Spagnol, S., D'Adamo, D., Pattiaratchi, C., 2001. Rapid, human-induced siltation of the macro-tidal Ord river estuary, western Australia. Estuar. Coast. Shelf Sci. 53, 717–732.
Xie, D.F., Wang, Z.B., Gao, S., de Vriend, H.J., 2009. Modeling the tidal channel morphodynamics in a macro-tidal embayment, Hangzhou Bay, China. Cont. Shelf Res. 29, 1757–1767.
Yu, Q., Wang, Y.W., Gao, S., Flemming, B., 2012. Modeling the formation of a sand bar within a large funnel-shaped, tide-dominated estuary: Qiantangjiang Estuary, China. Mar. Geol. 299–302, 63–76.
Zhang, G.J., Li, C.X., 1996. The fills and stratigraphic sequences in the Qiantangjiang incised paleovalley, China. J. Sediment. Res. 66, 406–414.